Transverse patterns in degenerate optical parametric oscillation and degenerate four-wave mixing

G. J. de Valcárcel,[1,*] K. Staliunas,[1,2,†] Eugenio Roldán,[1] and V. J. Sánchez-Morcillo[1]
[1]*Department d'Òptica, Universitat de València, Dr. Moliner 50 E-46100 Burjassot, Spain*
[2]*Laboratory 4.42, Physikalisch Technische Bundesantstalt, Bundesalle 100, 38116 Braunschweig, Germany*
(Received 14 February 1996)

Transverse pattern formation in both degenerate optical parametric oscillation and degenerate four-wave mixing is considered both theoretically and numerically. In the limit of small signal detuning both systems are shown to be described by the real Swift-Hohenberg equation. Contrarily, for small signal and large pump detunings the Swift-Hohenberg equation is modified differently in both systems, by the appearance of additional nonlinear terms, which signal the existence of nonlinear resonances that are theoretically studied through the derivation of the amplitude equation for the roll pattern in both systems. Numerical analysis supports the theoretical predictions. [S1050-2947(96)07907-3]

PACS number(s): 42.65.Sf, 42.65.Yj

I. INTRODUCTION

When studying the spatiotemporal dynamics of a nonlinear system inside a resonator with flat mirrors from the theoretical viewpoint there exist two basic alternatives that complement each other. One of them is the study of some special patterns such as, e.g., rolls, rhomboids, or hexagons. The equations that govern the time evolution of the amplitudes of the different components (in the wave-number domain) of these patterns are called amplitude equations. The other approach consists in the reduction, under some limitations, of the original *microscopic* equations of the system to a unique (when possible) equation: the order-parameter equation (OPE). The derivation of this kind of equation is of great practical and fundamental importance, since the OPE allows a simplified treatment of the system space-time dynamics (not constrained to special cases as the amplitude equations) and also interconnects different pattern-forming systems (either optical, hydrodynamical, chemical, biological, etc.) [1]. In the field of nonlinear optics both approaches have been used since Coullet, Gil, and Rocca [2] offered a derivation of the Ginzburg-Landau equation in optics.

Optical parametric oscillation (OPO) has proven to be a rich system from the point of view of the spatiotemporal dynamics [3–8]. It is a particularly attractive system because of its relatively simple mathematical description and because of its technological and fundamental relevance. In particular, the work of Oppo and co-workers [3,4] has shown that rolls play a central role in the pattern formation in degenerate OPO (DOPO), and Lugiato and Grynberg [7] have related the emergence of spatial structures with the well-known capability of DOPO for generating squeezed states of light. In a recent work, Brambilla, Camesasca, and Oppo [5] have also shown the appearance of complicated dynamics when the Hopf bifurcation for large pump values is reached. Oppo and co-workers [6] have described the relative stability between rolls and other steady patterns such as rhomboids, hexagons, and even dodecagons. Finally, Staliunas [8] has discussed the derivation of OPE's for the singly and doubly resonant OPO and has obtained a complex Ginzburg-Landau equation for the first case and a Swift-Honhenberg type equation for the second case, similar to that obtained by Mandel, Georgiou and Erneux [9] for nascent optical bistability and by some of us for nascent two-photon optical bistability [10]. The treatment in [8] is based on a simple approach of the adiabatic elimination of variables. Here we derive the OPE's using mathematically rigorous techniques of multiscale expansions.

The reason for the parallel study of DOPO and degenerate four-wave mixing (DFWM) are the well-known similarities existing between both systems that have been revealed both in their temporal instabilities and in their quantum properties aspects.

The paper is organized as follows. In Sec. II we derive OPE's for DOPO and for DFWM for small signal detuning in the cases of moderate and large pump detuning. For moderate pump detuning the real Swift-Hohenberg equation (SHE) is obtained for both systems, revealing that DOPO and DFWM are isomorphic systems for pattern formation in this limit. As rolls are the basic pattern supported by the SHE, our derivation provides a basis for the understanding of the central role played by rolls in DOPO transverse dynamics. For large pump detuning we derive a modified SHE that contains additional nonlinear terms that signal the appearance of a nonlinear resonance that has a huge importance in the properties of both systems. In this second case the OPE's are different for DOPO and DFWM revealing that the mentioned isomorphism is limited to a restricted parameter range. In order to study this nonlinear resonance several amplitude equations for rolls are derived in Sec. III, corresponding to the cases of small and large pump detuning. An interpolated amplitude equation for rolls is given, which allows one to study the passage from regimes of negligible nonlinear resonance to those where the nonlinear resonance is fully appreciated. In Sec. IV a numerical analysis is carried out in order to illustrate the main conclusions following from the OPE's and the amplitude equations. Finally, in Sec. V the main conclusions are outlined.

*Electronic address: qoval@vm.ci.uv.es

†Electronic address: kestutis.staliunas@ptb.de

II. DERIVATION OF THE ORDER PARAMETER EQUATIONS

In this section we present the derivation of the OPE's for DOPO (Sec. II A) and DFWM (Sec. II B). In both cases we consider the limit of small signal detuning and leave to Appendix A the case of finite positive detuning.

A. Order parameter equations for DOPO

The microscopic equations for DOPO inside a resonator consisting of plane mirrors, in the paraxial approximation and mean-field limit, read [3]

$$\partial_t A_0 = \gamma_0[-(1+i\Delta_0)A_0 + E' - A_1^2 + ia_0\overline{\nabla^2}A_0], \quad (1a)$$

$$\partial_t A_1 = \gamma_1[-(1+i\Delta_1)A_1 + A_1^* A_0 + ia_1\overline{\nabla^2}A_1], \quad (1b)$$

where $A_0(\overline{x,y,t})$ and $A_1(\overline{x,y,t})$ are the normalized slowly varying complex amplitudes of the pump and signal fields, respectively. The external coherent field has a normalized amplitude E' and oscillates at a frequency ω_L. Two longitudinal modes of the resonator of frequencies ω_0 and ω_1 are assumed to be close to ω_L and $\omega_L/2$. $\Delta_0=(\omega_0-\omega_L)/\gamma_0$ and $\Delta_1=(2\omega_1-\omega_L)/2\gamma_1$ are the detunings, where γ_0 and γ_1 are the cavity decay rates for each mode. $a_0=c/2k_z\gamma_0$ and $a_1=c/k_z\gamma_1$ are the diffraction parameters (k_z is the longitudinal wave vector of the external field). Finally, $\overline{\nabla^2}$ represents the transverse Laplacian operator referred to the spatial coordinates $(\overline{x,y})$.

The validity limits of Eqs. (1) are discussed in detail in Refs. [3,4]. The more restrictive approximation is the single-longitudinal mode operation for the subharmonic (that approximation usually holds for the pump wave because of the use of an external cw injection) since the relatively broad phase synchronization line for DOPO (10^9–10^{12} Hz) forces the length of the resonator to be correspondingly small (few millimeters and less).

In order to simplify as much as possible the forthcoming calculations it is convenient to rescale time and space coordinates as

$$\tau=\gamma_1 t, \quad x=\overline{x/}\sqrt{a_1}, \quad y=\overline{y/}\sqrt{a_1}, \quad (2)$$

and to introduce new fields, E,X, and Y through the changes

$$A_0=E+(1-i\Delta_0)X, \quad A_1=\sqrt{1+\Delta_0^2}Y, \quad E'=(1+i\Delta_0)E. \quad (3)$$

The inclusion of a factor involving Δ_0 in the definition of all three fields prevents them from growing to infinity as Δ_0 increases in modulus. This greatly simplifies the study of the large Δ_0 limit, and also has the advantage that the threshold for signal generation becomes Δ_0 independent, as will be seen. In this way Eqs. (1) become

$$\partial_\tau X = -\gamma(1+i\Delta_0)(X+Y^2) + i\tfrac{1}{2}\nabla^2 X, \quad (4a)$$

$$\partial_\tau Y = -(1+i\Delta_1)Y + [E+(1-i\Delta_0)X]Y^* + i\nabla^2 Y, \quad (4b)$$

where ∇^2 is the Laplacian operator referred to the new spatial coordinates (x,y), and $\gamma=\gamma_0/\gamma_1$. In the following E is taken to be real and uniform in space. In writing Eqs. (4) the relation $a_1\gamma_1=2a_0\gamma_0$ has been taken into account.

Equations (4) have the trivial homogeneous solution

$$X=Y=0, \quad (5)$$

whose linear stability analysis against space-dependent perturbations of wave vector $\mathbf{k}$ yields the eigenvalues

$$\lambda_{1\pm}(k) = -1 \pm \sqrt{E^2-(\Delta_1+k^2)^2},$$

$$\lambda_{0\pm}(k) = -\gamma[1 \pm i(\Delta_0+k^2/2\gamma)], \quad (6)$$

with $k^2=\mathbf{k}\cdot\mathbf{k}$. λ_0 and λ_1 are the growth exponents of X (pump field) and Y (signal field), respectively (they have this simple meaning due to the structure of the stability matrix, which decouples X and Y). λ_0 always has a negative real part, while λ_1 becomes positive for pump amplitude values $E \geqslant E_B(k)$ with

$$E_B(k)=\sqrt{1+(\Delta_1+k^2)^2}, \quad (7)$$

thus indicating the existence of a bifurcation at $E_B(k)$.

This function (7) has a minimum at $k=k_0$ with

$$k_0=0 \quad \text{for} \quad \Delta_1>0, \quad (8a)$$

$$k_0=\sqrt{-\Delta_1} \quad \text{for} \quad \Delta_1<0. \quad (8b)$$

This second case is the most interesting one since the nonzero value of k_0 implies the formation of nonuniform spatial structures (Turing patterns) above the bifurcation threshold (7) and we will concentrate on this case. At $k=k_0$ the pump threshold reduces to $E_B(k_0)\equiv E_0$ with

$$E_0=\sqrt{1+\Delta_1^2} \quad \text{for} \quad \Delta_1>0, \quad (9a)$$

$$E_0=1 \quad \text{for} \quad \Delta_1<0, \quad (9b)$$

which is the threshold for DOPO generation.

For deriving order-parameter equations we will next make asymptotic expansions of the fields in terms of a smallness parameter ε. For doing that it is necessary to know how a small increase in the pump amplitude above the threshold value

$$E=E_0+\varepsilon^2 E_2 \quad (10)$$

influences the largest eigenvalue λ_{1+} (6). Substitution of (10) into (6) leads to

$$\lambda_{1+}(k) = -1+\sqrt{E_0^2-(\Delta_1+k^2)^2} + \frac{E_0 E_2}{\sqrt{E_0^2-(\Delta_1+k^2)^2}}\varepsilon^2 + O(\varepsilon^4). \quad (11)$$

Particularly, the largest λ is $\lambda_{1+}(k_0)=E_2\varepsilon^2$ for both signs of Δ_1, which suggests the introduction of a slow time scale

$$T=\varepsilon^2\tau. \quad (12)$$

We analyze the case of negative detuning here and leave the case of positive detuning to Appendix A. The derivation of an OPE requires that the Laplacian operator does not appear

in the asymptotic expansion at $O(\varepsilon)$, since in that case only special spatial structures can be treated. Thus we impose that the spatial part scales as

$$\nabla^2=\varepsilon\nabla_1^2. \tag{13}$$

Since for $\Delta_1<0$ $k_0\neq 0$ [Eq. (8b)], a necessary condition for the Laplacian operator to be regarded as a small operator is $k_0=O(\varepsilon^{1/2})$, or, equivalently,

$$\Delta_1=\varepsilon\delta_1. \tag{14}$$

This restriction turns out to be sufficient for ensuring that the width (in **k** space) of unstable modes is also $O(\varepsilon^{1/2})$, as can be easily deduced from Eq. (11), and so for ensuring that (13) holds.

Finally, let us notice that the order of Δ_0 is not fixed by the linear stability analysis. Then, we will consider two different cases for deriving the order-parameter equations: that Δ_0 be of order one and that Δ_0 be of order ε^{-1}.

1. Case of finite pump detuning: Real Swift-Hohenberg equation

Now we proceed to make an asymptotic expansion of Eqs. (1) around the homogeneous steady-state solution (5):

$$X=\sum_{n=1}^{\infty}\varepsilon^n X_n, \quad Y=\sum_{n=1}^{\infty}\varepsilon^n Y_n. \tag{15}$$

Let us consider the case of small signal detuning. So we substitute Eqs. (10) and (15) into Eqs. (4), apply the scalings (12)–(14), and solve at the successively increasing orders of ε. At order ε we find

$$X_1=0, \tag{16a}$$

$$Y_1=Y_1^*, \tag{16b}$$

so Y_1 is real. At order ε^2 we obtain, taking into account Eqs. (16),

$$X_2=-Y_1^2, \tag{17a}$$

$$Y_2-Y_2^*=-i(\delta_1-\nabla_1^2)Y_1. \tag{17b}$$

At order ε^3 we only need the equation for the signal field that, taking into account Eqs. (16) and (17a), reads

$$\partial_T Y_1=Y_3^*-Y_3-i(\delta_1-\nabla_1^2)Y_2+E_2Y_1+(1-i\Delta_0)Y_1^3. \tag{18}$$

Finally, by adding Eq. (18) with its complex conjugate and using (17b) we obtain

$$\partial_T Y_1=E_2Y_1-Y_1^3-\tfrac{1}{2}(\delta_1-\nabla_1^2)^2Y_1, \tag{19}$$

which can be written in terms of the initial parameters and of the signal amplitude Y to leading order in ε as

$$\partial_\tau Y=pY-\tfrac{1}{2}(\Delta_1-\nabla^2)^2Y-Y^3, \tag{20a}$$

$$p=E-1. \tag{20b}$$

Equation (20) is the real Swift-Hohenberg equation (SHE) [11], and describes the space-time dynamics of DOPO close to threshold under small detuning conditions.

2. Case of large pump detuning: Nonlinear resonance

We consider next the case of small signal detuning as above but now with

$$\Delta_0=\varepsilon^{-1}\delta_0. \tag{21}$$

Following the same procedures as in the preceding subsection, from the first and second orders in ε one obtains again Eqs. (16), (17a), and

$$X_3=-2Y_1Y_2, \tag{22a}$$

$$Y_2-Y_2^*=i(\delta_1-\nabla_1^2-\delta_0Y_1^2)Y_1. \tag{22b}$$

Finally, at third order one gets, after Eqs. (21) and (22a) have been used,

$$\partial_T Y_1=-Y_3+Y_3^*-i\delta_1Y_2+i\delta_0(2Y_2+Y_2^*)+E_2Y_1-Y_1^3+i\nabla_1^2Y_2. \tag{23}$$

By adding Eq. (23) to its complex conjugate and by using Eq. (22b) one finally finds

$$\partial_\tau Y=pY-\tfrac{1}{2}(\Delta_1-\nabla^2-\Delta_0Y^2)^2Y-Y^3, \tag{24}$$

to leading order in ε. It is remarkable that Eq. (24) contains a fifth-order nonlinearity ($-\Delta_0Y^5/2$) and also appears a differential nonlinearity ($-\Delta_0Y^2\nabla^2Y/2$), which produce a nonlinear resonance. This equation was first obtained by one of us in Ref. [8] by assuming conditions for adiabatic elimination of the pump field in the DOPO. Notice that one can think of Eq. (24) as the OPE for DOPO for small signal detuning and close to threshold, independently of the magnitude of the pump detuning: if Δ_0 is moderate (say order 1) then the term Δ_0Y^2 is $O(\varepsilon^2)$ and thus negligible with respect to the other terms [in this way the SHE Eq. (21) is recovered]. Incidentally, we note that in the absence of transverse effects ($\nabla^2\to 0$) Eq. (24) reproduces the well-known bistability between the trivial solution and the DOPO solution for $\Delta_0\Delta_1>1$.

B. Order-parameter equations for DFWM

The simplest microscopic model for DFWM [12] inside a resonator consisting of plane mirrors, including diffraction, can be written as

$$\partial_t A_0=\gamma_0[-(1+i\Delta_0)A_0+E'-A_0^*A_1^2+ia_0\overline{\nabla^2}A_0], \tag{25a}$$

$$\partial_t A_1=\gamma_0[-(1+i\Delta_1)A_1+A_0^2A_1^*+ia_1\overline{\nabla^2}A_1]. \tag{25b}$$

Equations (25) describe the two-photon interaction between two fields A_0 (pump) and A_1 (signal) of the same frequency ω_L with a nonlinear $\chi^{(3)}$ medium. A_0 and A_1 may differ, for instance, in their polarization. In Eqs. (25) the relation between diffractions is $a_1\gamma_1=a_0\gamma_0$, the signal detuning $\Delta_1=(\omega_1-\omega_L)/\gamma_1$, and the rest of symbols keep the

same meaning and definitions as in Eqs. (1). The same remarks that were made after Eqs. (1) regarding the validity of the model apply here.

It is again convenient to use the rescaled time and spatial coordinates defined in Eq. (2) as well as the rescaled and shifted variables defined in Eq. (3). The rescaled equations read

$$\partial_\tau X = -\gamma(1+i\Delta_0)\{X+[E+(1+i\Delta_0)X^*]Y^2\}+i\nabla^2 X, \tag{26a}$$

$$\partial_\tau Y = -(1+i\Delta_1)Y+[E+(1-i\Delta_1)X]^2Y^*+i\nabla^2 Y. \tag{26b}$$

It can be seen that the linear stability analysis if Eqs. (26) leads to the same result as for the DOPO equations with the only difference being that E^2 must be replaced by E^4 and consequently the same scalings must be adopted for the DFWM. Thus we will not give details of the derivation since it is carried out by following the same lines that have been followed for the DOPO case. For the sake of brevity, we give the final result. For small signal detuning one obtains

$$\partial_\tau Y = 2pY-\tfrac{1}{2}(\Delta_1-\nabla^2)^2Y-2Y^3, \tag{27}$$

and for large pump detuning one obtains

$$\partial_\tau Y = 2pY-\tfrac{1}{2}(\Delta_1-\nabla^2-2\Delta_0Y^2)^2Y-2Y^3+\Delta_0^2Y^5, \tag{28}$$

with $p=E-1$ small. Both Eqs. (24) and (25) are valid to leading order in ε. Notice that Eq. (27) is isomorphic to Eq. (20) after change of the variables $Y\to Y/\sqrt{2}$ and $p\to p/2$ in Eq. (24). Thus, both DOPO and DFWM are isomorphic as pattern-forming systems when signal detuning is small. Contrarily, Eq. (28) is not isomorphic to Eq. (24) because of the presence of an additional fifth-order term [last term in the right-hand side of Eq. (28)], denoting that the isomorphism does not exist for arbitrary conditions. As will be shown below, this additional fifth-order term can cause the irregular behavior of (28) for large values of the pump parameter p or pump detuning Δ_0.

C. Discussion

The OPE's that we have derived in the previous subsections for both DOPO and DFWM suggest a number of straightforward conclusions. On the one hand, both systems are isomorphic for not too large pump detuning values, verifying in this case the real SHE [Eqs. (20) and (27)]. It is well known that the real SHE exhibits stable roll patterns for negative detuning, and that these rolls destabilize for nonresonant wave numbers through zigzag or Eckhaus instabilities (see, e.g., [1]). Thus, this result provides analytical support to the numerical observation of roll patterns by Oppo and co-workers [3,4]. In fact their results show that, for the DOPO, the validity of the prediction that the rolls are the basic stable pattern goes beyond the limits of applicability of the OPE, although other patterns can also be found [5,6]. This indicates the structural robustness of the OPE for DOPO, which is also illustrated by our numerical examples below.

For large values of the pump detuning, a modified SHE has been obtained, the modification consisting in the appearance of additional nonlinear terms [Eqs. (24) and (28)]. The isomorphism between DOPO and DFWM is no longer verified in this limit although their respective OPE's continue to be similar. Recall that Eq. (24) was obtained by one of us [8] by following an adiabatic elimination procedure. Here we have shown that this equation is valid independently of the values of the relaxation constants. These equations have a special interest since the presence of the additional higher-order nonlinearities signals the existence of a nonlinear resonance in the system which is investigated in the next section for the roll pattern.

Let us finally comment that along all the previous derivations the relative decay rate γ has been implicitly assumed to be $O(1)$, although we have checked that the derivations are also valid for arbitrarily large γ (that would correspond to the adiabatic elimination of the pump field). On the contrary, in the case $\gamma \leqslant O(\varepsilon)$ no OPE can be derived.

III. AMPLITUDE EQUATIONS FOR ROLLS

In this section we derive the amplitude equation for rolls for both DOPO and DFWM. We make this derivation starting from the microscopic equations and not with the OPE's. The main reason for deriving the amplitude equation from the microscopic equations is that we need not limit ourselves to the case of small signal detuning and thus a more general amplitude equation can be obtained if one derives it starting from the microscopic equations. In the following the signal detuning Δ_1 is assumed to be negative since only in that case may nonuniform patterns appear [Eq. (8b)].

For deriving the amplitude equation for rolls we assume a small value of the pump above threshold [Eq. (10)] and introduce into the microscopic equations (4) an expansion of the signal field of the form

$$Y=(\Psi e^{ik_0x}+\Psi^* e^{-ik_0x})+O(\varepsilon^2), \tag{29a}$$

$$\Psi=\varepsilon B, \tag{29b}$$

that is a one-dimensional (1D) structure consisting of rolls of spatial frequency k_0 oriented parallel to the y direction to leading order in ε when the amplitude B is constant. Nevertheless apart from the k_0 mode (the most unstable mode) other modes with spatial frequencies close to k_0 have a positive eigenvalue [see Eq. (11)]. As usual [13], in the vicinity of $\mathbf{k}_0=(k_0,0)$ the domain of these amplified k modes has a width $\delta k_\parallel$ along the direction parallel to $\mathbf{k}_0$ of order ε/k_0 (provided that the pump above threshold is of order ε^2), and a width $\delta k_\perp$ along the direction perpendicular to $\mathbf{k}_0$ of order $\sqrt{\varepsilon}$, as can be deduced from Eq. (11). Then we must introduce a multiple spatial scaling in order to take into account the appearance of very different spatial scales. Of course this multiple spatial scaling will be different depending on the order of magnitude of the signal detuning Δ_1, which governs the magnitude of k_0, and thus that of $\delta k_\parallel$.

For $\Delta_1=O(1)$ $[k_0=O(1)]$, the appropriate multiscale expansion is

$$x\to x+\varepsilon^{-1}u, \tag{30a}$$

$$y \rightarrow \varepsilon^{-1/2} v, \tag{30b}$$

that leads to the expansion of the Laplacian operator

$$\nabla^2 = L_0 + \varepsilon L_1 + \varepsilon^2 L_2, \tag{31a}$$

$$L_0 = \partial_x^2, \tag{31b}$$

$$L_1 = 2\partial_x \partial_u + \partial_v^2, \tag{31c}$$

$$L_2 = \partial_u^2. \tag{31d}$$

Alternatively for $\Delta_1 = O(\varepsilon^{-1})$ $[k_0 = O(\varepsilon^{-1/2})]$ the appropriate multiscale expansion is

$$x \rightarrow \varepsilon^{-1} x_0 + \varepsilon^{-3/2} u, \tag{32a}$$

$$y \rightarrow \varepsilon^{-1/2} v, \tag{32b}$$

that leads to the expansion of the Laplacian operator

$$\nabla^2 = \varepsilon^{-1} L_{-1} + \varepsilon L_1 + \varepsilon^3 L_3, \tag{33a}$$

where

$$L_{-1} = \partial_{x_0}^2, \tag{33b}$$

L_1 is given by Eq. (31c) and L_3 has the same expression as L_2 in Eq. (31d).

Apart from the order of magnitude of Δ_1 we must also distinguish between two basic possibilities for the order of magnitude of the pump detuning Δ_0 (order one or order $1/\varepsilon$) related to the absence or existence of a nonlinear resonance, as suggested by the previous OPE's. Consequently, we can derive several different amplitude equations depending on the orders of magnitude of both detunings. Although none of the amplitude equations will be valid for all the possible orders of magnitude of the signal and pump detunings, it will be possible to construct by interpolation an amplitude equation that is valid in all the limits of interest.

A. Amplitude equation for rolls in DOPO

As shown in Appendixes B and C, the amplitude equation for rolls in DOPO reads, in terms of unscaled variables,

$$\begin{aligned}\partial_\tau \Psi(x,y) = {} & p\Psi - (2+\alpha^2)|\Psi|^2\Psi - \tfrac{1}{2}\Delta_0^2(2+\alpha)^2|\Psi|^4\Psi \\ & - \tfrac{1}{2}L^2\Psi - \tfrac{1}{2}\Delta_0[(2-\alpha)\Psi^2 L^*\Psi^* + 2\alpha|\Psi|^2 L\Psi \\ & + (2+\alpha)L(|\Psi|^2\Psi)],\end{aligned} \tag{34a}$$

where Ψ is defined by (29a), and

$$\alpha = \left(\frac{1+\Delta_0^2}{1+(\Delta_0 - 2\Delta_1/\gamma)^2}\right)^{1/2}, \tag{34b}$$

$$L = 2ik_0\partial_x + \partial_y^2. \tag{34c}$$

Equation (34a) is an interpolation of the amplitude equations obtained in the cases Δ_0 and Δ_1 of order one [Eq. (B5) in Appendix B] and Δ_0 and Δ_1 of order $1/\varepsilon$ [Eq. (C9) in Appendix C] and is valid for any value of the detunings, whenever $p = E - 1$ is small. The same Eq. (34a) is obtained from the Swift-Hohenberg equation (20) and its generalization to nonlinear resonance, Eq. (24), when the corresponding limits are taken in Eqs. (34a) and (34b).

We can look now for an exact stationary solution of Eq. (34a). Given the rotational invariance of the problem we choose to study a roll oriented along the y direction:

$$\Psi(x,y) = \psi e^{ikx}, \tag{35}$$

taking ψ as a real quantity without loss of generality. One easily gets

$$\begin{aligned}&(2+\alpha)^2\Delta_0^2\Psi^4 + 2[2+\alpha^2 - 2\Delta_0(2+\alpha)k_0 k]\Psi^2 \\ &\quad - 2(p - 2k_0^2 k^2) = 0.\end{aligned} \tag{36}$$

This stationary solution can be shown to coincide with the *resonant* roll solution ($k=0$) derived in [3], for not large Δ_0.

In Figs. 1(a) and 1(b) the squared amplitude ψ^2 of the roll solution, as given by (36), is plotted vs k for different values of the pump p given in the figures. For low pump detunings [$\Delta_0 = 0$ in Fig. 1(a)] the usual dependence as observed in the Swift-Hohenberg model [1] is noted. Nevertheless increasing pump detuning (in modulus) causes the nonlinear resonance to appear in Fig. 1(b) ($\Delta_0 = -5$): the maximum emission is not obtained for $k=0$ (linear resonance) but varies as the pump increases; the larger the pump, the further the maximum is located from the linear resonance. For positive Δ_0 the behavior is similar to that displayed in Fig. 1(b) but with the curves extending towards positive k's consistent with OPE (24): since the linear operator [the second one on the right-hand side (rhs) of (24)] is negative (it is a squared quantity affected by a minus sign) the maximum emission will be reached when it is null, and this depends on the sign of Δ_0. With the aim of illustrating this point in a simple but not rigorous way we can substitute the Laplacian in (24) by $-(k_0+k)^2$, where $k_0^2 = -\Delta_1$, assuming that the largest contribution to it is due to a pure roll of spatial frequency (k_0+k). Then the linear operator is approximately written as $-(1/2)[-k_0^2 + (k_0+k)^2 - \Delta_0 Y^2]^2$ and one concludes that the squared amplitude of the roll at its maximum $\psi_{\max}^2 \propto [(k_0+k)^2 - k_0^2]/\Delta_0$. Thus Δ_0 and k must have the same sign at the maximum of ψ^2. This simple reasoning is consistent with the actual value of the wavenumber k for which the intensity ψ^2 is maximum. It is simple to obtain from Eq. (36) that the maximum of ψ^2 is given by

$$\psi_{\max}^2 = \frac{p}{2+\alpha^2} \tag{37a}$$

and is reached at $k = k_{\mathrm{NLR}}$, with

$$k_{\mathrm{NLR}} = \frac{2+\alpha}{2(2+\alpha^2)}\frac{p\Delta_0}{k_0}, \tag{37b}$$

thus k and Δ_0 must have the same sign at the maximum of ψ^2. As a further illustration of the nonlinear resonance we plot in Fig. 1(c) the dependence of the roll intensity ψ^2 as a function of pump p for different values of the spatial fre-

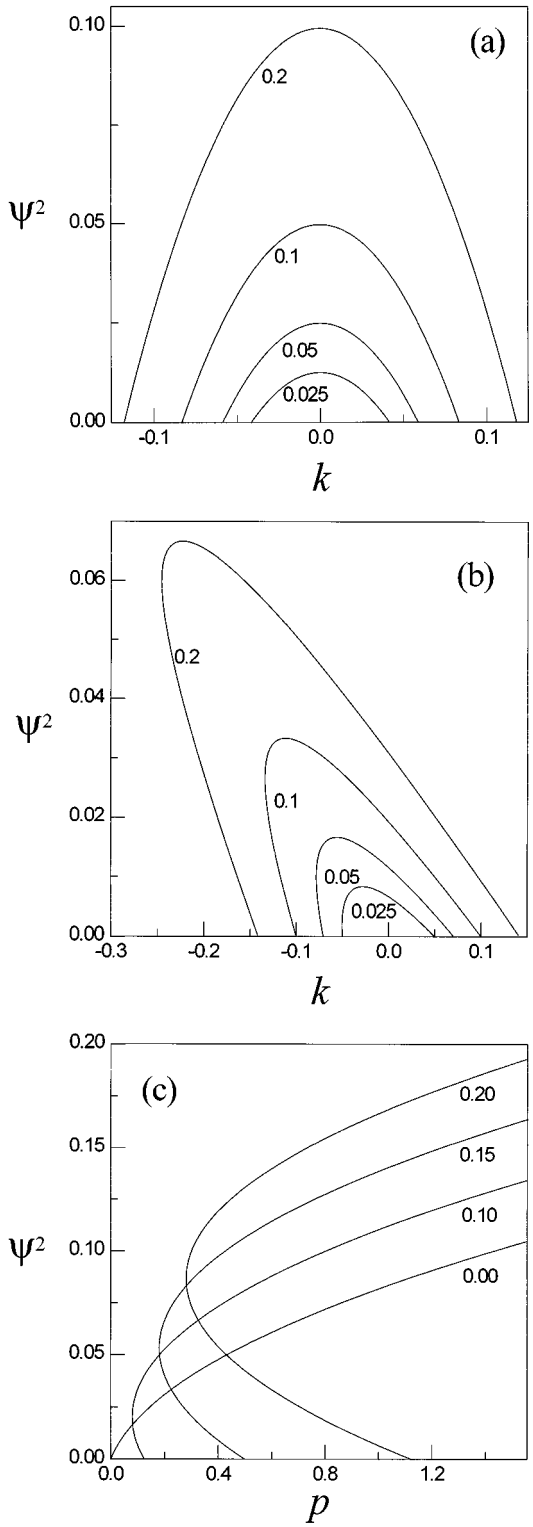

FIG. 1. (a) Dependence of the DOPO roll intensity ψ^2 [Eq. (36)] on k for resonant pump ($\Delta_0=0$), $\Delta_1=-5$ and the four values of the pump above threshold p given in the figure. (b) As in (a) but for $\Delta_0=-5$. (c) Dependence of ψ^2 with p for the same parameters as in (b) and the four values of k given in the figure.

quency k indicated in the figure, for the same parameters as in Fig. 1(b). Except for the linearly resonant roll ($k=0$) the intensities of the rest of the rolls show two branches, the lower one always being unstable. It is to be remarked that no roll solution exists for $p<0$ thus preventing the existence of bistability between the trivial and the roll solutions, as can be deduced from Eq. (36).

B. Amplitude equation for rolls in DFWM

In the case of DFWM the amplitude equation for rolls reads, as shown in Appendixes D and E, in terms of unscaled variables,

$$\partial_\tau \Psi(x,y) = 2p\Psi - 2(2+\beta^2)|\Psi|^2\Psi - 4\Delta_0^2(1+\beta)|\Psi|^4\Psi - \tfrac{1}{2}L^2\Psi - \Delta_0[(2-\beta)\Psi^2 L^*\Psi^* + 2\beta|\Psi|^2 L\Psi + (2+\beta)L(|\Psi|^2\Psi)], \tag{38a}$$

where

$$\beta = \left(\frac{1+\Delta_0^2}{1+(\Delta_0-4\Delta_1/\gamma)^2}\right)^{1/2}, \tag{38b}$$

and L is given by Eq. (34c). As before, Eq. (38) is an interpolation of the amplitude equations obtained in the cases Δ_0 and Δ_1 of order one [Eq. (D3) in Appendix D] and Δ_0 and Δ_1 of order $1/\varepsilon$ [Eq. (E7) in Appendix E] and is valid, in principle, for any value of the detunings.

Again we look now for the stationary solution of Eq. (38a):

$$2(1+\beta)\Delta_0^2\psi^4 + [2+\beta^2-2\Delta_0(2+\beta)k_0k]\psi^2 - (p-k_0^2k^2) = 0. \tag{39}$$

Although Eq. (39) looks very similar to the amplitude equation Eq. (36) for rolls in DOPO, their solutions differ qualitatively for some parameter sets. Figure 2 shows the predictions of Eq. (39). For small values of the pump detuning Δ_0 the same behavior as in the DOPO case [Fig. 1(a)] is observed, while for increasing Δ_0 (in modulus) qualitative differences are observed. In Fig. 2(a) we plot the roll intensity ψ^2 as a function of the roll spatial frequency k for several values of the pump p indicated in the figure and $\Delta_0=\Delta_1=-5$. If for small pumps the nonlinear resonance manifests itself in a way similar to the DOPO case [Fig. 1(b)] for larger pumps (but as small as 0.02) the prediction of Eq. (39) clearly fails since it gives rise to divergent solutions for negative k's. Moreover, any ''sensible'' curve in Fig. 2(a) has a nonsense companion (e.g., the upper-left curves corresponding to $p=0.013$ and 0.016). These spurious curves exist even for smaller pumps (e.g., for $p=0.005$, not shown in the figure) and correspond to large negative values of k and large intensities, thus not fulfilling the smallness requirements assumed in the derivation of the amplitude equation (39). We can understand this negative result as a direct consequence of the structure of the OPE for DFWM (28). Differently from the OPE for DOPO [Eq. (24)] in the DFWM case there exists an additional fifth-order nonlinearity [last term on the rhs of Eq. (28)] which is positive and destabilizes the solution for sufficiently large pump p and pump

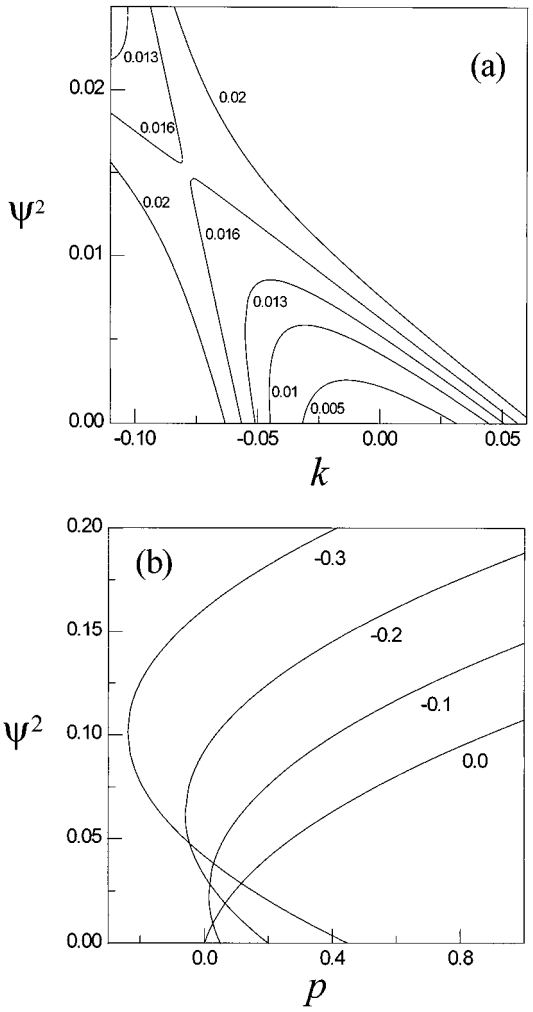

FIG. 2. (a) Dependence of the DFWM roll intensity ψ^2 [Eq. (38)] on k for $\Delta_0=-5$, $\Delta_1=-5$ and the four values of the pump above threshold p given in the figure. (b) Dependence ψ^2 with p for the same parameters as in (a) and the four values of k given in the figure.

detuning Δ_0. Thus we conclude that both the OPE and the amplitude equation for rolls in DFWM are of limited validity.

Let us finally discuss the phenomenon of bistability between rolls and the trivial solution in DFWM. In Fig. 2(b) we plot the pump dependence of the roll intensity as given by Eq. (38) for the parameters of Fig. 2(a) and several values of k indicated in the figure. It is evident that roll solutions exist below the DFWM generation threshold ($p=0$), differently from the DOPO case. Nevertheless this bistability occurs for large values of $|k|$ thus corresponding to badly behaved resonance curves, as discussed above in Fig. 2(a). So it is not clear whether these bistable states can actually be found in DFWM.

Up to here we have elaborated on a theoretical approach to the description of both DOPO and DFWM. In the next section we show numerical results obtained by integration of the microscopic equations, illustrating the theoretical predictions and also showing some other features.

IV. NUMERICS

We have performed a series of numerical experiments in order to test the predictions derived from the OPE's and amplitude equations derived in the preceding section for DOPO and DFWM. We have numerically integrated the initial set of microscopic equations for both DOPO and DFWM by using the split-step technique. In this method the local terms (pump, losses, nonlinear coupling) are calculated in the space domain while the nonlocal terms (diffraction for all waves) are calculated in the spatial wave-vector domain. A fast Fourier transformation is used to shift from the space to the spatial wave-number domain in every time step. Several spatial grids were used ranging from (64×64) to (128×128). Periodic boundaries were used in all the numerical calculations. In order to have a larger flexibility in the numerical calculations we have integrated the original equations (1) for DOPO and (25) for DFWM, instead of the normalized ones, Eqs. (4) and (26) respectively, which are more suited for theoretical treatments. Thus, in this section the wave numbers are referred to the unscaled space variables, and the value of the diffraction coefficients a_0 and a_1 must be specified. In order to avoid misunderstandings we denote by K a generic wave number and by K_0 the wave number corresponding to the linear resonance.

We built the numerical experiments with the intention of checking the following aspects of the OPE's.

(i) Show that the roll pattern of the initial DOPO microscopic equations behave similarly to the rolls of the SHE. For this purpose we numerically calculated the stability limits of the rolls in DOPO, and compared with those for rolls in the SHE. As in the SHE, we have found that the rolls lose their stability through zigzag and Eckhaus instabilities.

The stability analysis of the rolls only provides information about where the rolls are stable or not in the parameter space, but it says little about the final states after the occurrence of the instability. We also investigated numerically the ''post-zigzag'' and the ''post-Eckhaus'' states.

(ii) As found recently by Price and co-workers [14] the purely cubic SHE, besides the rolls, also supports stable hexagons. These hexagons are characterized by the presence of a plane-wave component ($\mathbf{k}=\mathbf{0}$) in addition to the three-roll components with an angle of $2\pi/3$ in between. We have also found these hexagons by direct numerical integration of the DOPO equations. We show that there exists a domain of bistability between the hexagon and the roll patterns in the DOPO, exactly as follows from the analysis of SHE [14].

Regarding the DFWM, its isomorphism with DOPO close to the generation threshold for small pump detuning indicates that the behavior of both systems must be similar. In our numerical analysis of DFWM the same patterns and phenomena occurring in DOPO were observed: rolls, Price hexagons, Eckhaus and zigzag instabilities. Thus the presentation of these calculations for DFWM would be simply a repetition of the results for DOPO. For this reason we will only present some numerical results emphasizing not the similarities, but the differences between these systems:

(iii) As shown in Sec. III there is a nonlinear resonance in the spatial wave-number domain for both DOPO and DFWM when the pump detuning is large enough. This nonlinear

resonance means that the value of the resonant wave number for a particular roll solution depends on the amplitude of that roll. We have checked this particular form of the resonance curve by integrating numerically the microscopic equations for large pump detuning. We have found good correspondence with the curves of the nonlinear resonance that follow from the amplitude equations for rolls [Eqs. (36) and (38)]. The comparison of the nonlinear resonance curves for DOPO and DFWM shows that the already noted similarity between both systems is limited and new phenomena appear.

A. Rolls and their instabilities

The stability of the roll pattern in DOPO is a quite well established fact [3,4]. We have also found that rolls are the very basic pattern of DOPO in most of the numerical experiments. This fact already allows one to expect some further relation between the DOPO and the SHE (given that the basic solutions of the SHE are rolls), not only restricted to the small signal detuning limit where the SHE was derived for DOPO. The next step in checking this DOPO-SHE analogy is to compare the stability region of the rolls in both systems of equations. We concentrate on the resonant pump case $\Delta_0=0$ since in this limit the nonlinear resonance is not expected.

The roll solution to the SHE

$$Y=(\psi e^{iKx}+\psi^* e^{-iKx})+O(\varepsilon^2), \tag{40}$$

with $\psi=O(\varepsilon)$ and $p=O(\varepsilon^2)$, has an intensity $\psi^2=p-(K-K_0)^2$ [1]. In particular, steady states exist whenever $(K-K_0)^2\leqslant p$, and the equality defines the so-called neutral stability curve. In the optical context we have $K_0^2=-\Delta_1/a_1$ (the resonant roll), and thus the intensity reads

$$\psi^2=p-(K-\sqrt{-\Delta_1/a_1})^2, \tag{41}$$

so its maximum value $\psi^2_{\max}=p$ is reached at $K=K_0$. The standard analysis of rolls in the SHE [1] yields that they are Eckhaus-unstable if

$$p>(K-K_0)^2>p/3, \tag{42a}$$

or, alternatively, if

$$\psi^2<2p/3=2\psi^2_{\max}/3. \tag{42b}$$

In the numerical integrations the allowed values for the wave numbers K are discrete, so in order to check the above predictions in a continuous way it is more convenient to perform the integrations by fixing K and varying the signal detuning Δ_1 (or, equivalently, varying $K_0=\sqrt{-\Delta_1/a_1}$). In order to fix K an initial seed of the form ($Y=\cos/(Kx)$, $X=0$) is used. Thus, according to the SHE result rolls must be Eckhaus-unstable when signal detuning Δ_1 is large enough for their intensity ψ^2 [Eq. (41)] to verify condition (42b). As is well known, the Eckhaus instability occurs equally for the rolls with wave numbers shorter ($K<K_0$) or larger ($K>K_0$) than the resonant one. Nevertheless, in the former case the zigzag instability is also present [1] and so, in order to check the Eckhaus instability alone we have initially restricted ourselves to a pure 1D case (this is easily done in the equations by simply canceling the second derivative with respect to the y coordinate).

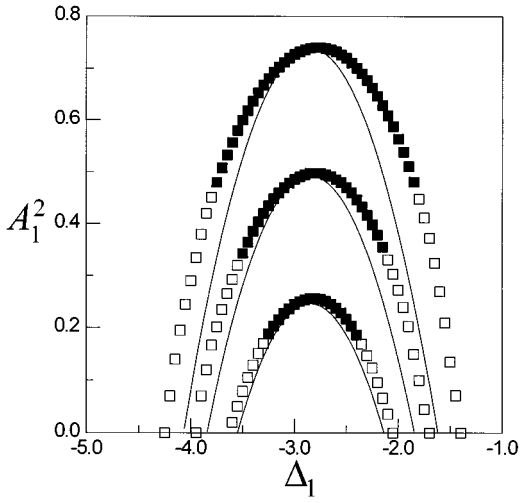

FIG. 3. The total signal field intensity of one dimensional roll pattern as a function of the signal detuning Δ_1. Empty (filled) squares indicate unstable (stable) rolls. The values of the pump parameter are, from the lower to the upper curve, $p=0.25$, 0.5, and 0.75. The analytical results [obtained from Eq. (36)] are represented by the solid lines. The rest of the parameters are $a_1=0.002$, $a_0=a_1/2$, $\Delta_0=0$, and $\gamma_0=\gamma_1=1$.

In Fig. 3 the stability analysis of the rolls is presented. Keeping a constant value of the pump p and a constant value of K (which was taken to be the resonant mode for $\Delta_1=-2.842\,45$), we slowly changed the value of the signal detuning (and, consequently, the value of K_0) and measured the intensity of the rolls. We found that the rolls were stable for any K (when they existed) if the fields were not perturbed during the calculation. These perturbation-free computations allowed us to plot the dependence of the intensity of the roll patterns on the signal detuning both in Eckhaus-stable (filled squares) and unstable (open squares) domains. To observe the instability of the rolls, a small external perturbation is necessary, since the split-step technique yields no noise in the spatial wave-number domain except maybe on the spatial subharmonics. The external perturbations seed the possible Eckhaus instability. As the filled squares in Fig. 3 indicate, the rolls are Eckhaus-stable for $\psi^2>2\psi^2_{\max}/3ca$. For large enough detuning (positive and negative), i.e., when the amplitude of rolls is $\psi^2<2\psi^2_{\max}/3ca$, the Eckhaus instability occurs. We thus find that the numerically calculated instability limits coincide well with those following from the theoretical analysis not only for small pump values, but also for quite moderate ones (a few times over threshold, see caption).

For the sake of comparison the analytically calculated resonance curves of the rolls [Eq. (36)] (solid lines) are also shown. A surprisingly good correspondence is observed [note the values of the pump parameter and the large variations of the detuning Δ_1 with respect to its central (resonant) value]. The main differences are quantitative and concern the fact that in general the numerically calculated roll-intensity versus detuning curves are broader than those obtained from the amplitude equation. This fact signals the presence of

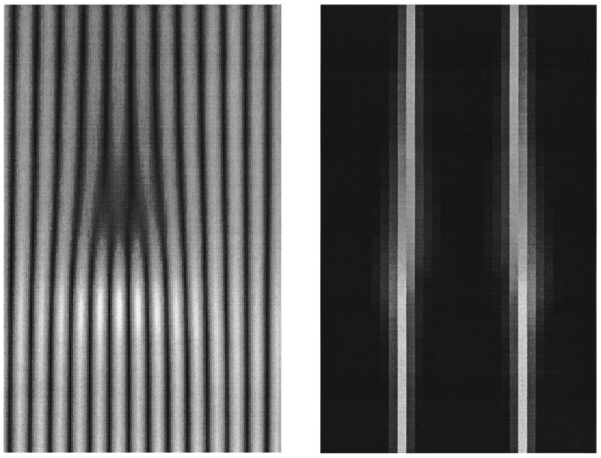

FIG. 4. Scenario of Eckhaus instability for one-dimensional rolls. (Left) temporal evolution of the spatial distribution of the signal field, (right) its spatial Fourier spectra. The spatial coordinate is horizontal (128 pixels) and the time runs from top to bottom over $\Delta t = 3.5$. $p = 0.75$, $\Delta_1 = -3.9$ and the rest of the parameters as in Fig. 3

some ''innocent'' higher-order nonlinearities in DOPO, which bring some quantitative discrepancies, but do not lead to any qualitative change.

We note that, in agreement with the SHE prediction [15], the Eckhaus instability in DOPO manifests itself through a transient in which the initial off-resonant roll pattern is substituted by a different roll pattern that is closer to resonance (although, in general, not necessarily by the resonant roll). Figure 4 illustrates the scenario of this process of substitution, mediated by the Eckhaus instability.

As commented above, in the 2D case in addition to the Eckhaus instability there exists another type of instability for the rolls: the zigzag instability. From the analysis of the SHE [1] we know that the zigzag instability affects any roll solution with a wave vector shorter than the resonant one: $K < K_0$. However, little is known about the ''post-zigzag'' states even in the SHE. It is not clear in general whether the zigzags are stable solutions, or they are only an intermediate solution until the system reaches a different roll pattern that is closer to the resonance.

We cannot give a definitive answer to this question. Our numerical simulations indicate that zigzagged rolls in DOPO are stable if their original wave number K is close to the zigzag instability boundary $K = K_0$ (but inside of the zigzag instability domain) and that they are unstable when K falls deep inside the zigzag instability domain, thus playing only an intermediate role in the last case.

The scenario we have observed in the case of unstable zigzagged rolls is the following: (i) the appearance of two *resonant* roll components $\mathbf{K}_{\pm 1} = (K, \pm K_{zz})$, with $|\mathbf{K}_{\pm 1}| = K_0$ (or, equivalently $K_{zz}^2 = K_0^2 - K^2$), due to the zigzag mechanism, in addition to the initial nonresonant roll $(K,0)$; (ii) the decay of the initial roll due to competition with the growing resonant components $\mathbf{K}_{\pm 1}$ and the growth of other weak ''harmonics'' $\mathbf{K}_n = (K, nK_{zz})$, $n = \pm 2, \pm 3, \ldots$; and (iii) the competition between the two resonant components $\mathbf{K}_{\pm 1}$, and the survival of only one of them, thus the original roll of spatial frequency K being replaced by a *resonant* roll with different orientation with respect to the original one. The series of plots in Fig. 5 illustrates this scenario.

Figure 6 shows an example of a stable zigzagged roll. In all the cases in which we have found these stable zigzags not only were the two strong components at $\mathbf{K}_{\pm 1}$ present but also relatively strong components at $\mathbf{K}_{\pm 2}$, at least, were apparent, differently from the transient scenario described above in which these ''harmonics'' were much weaker (compare Fig. 6 with Fig. 5). This leads to the suggestion that the presence of at least five relatively strong roll components is necessary for stabilizing the zigzags. This would happen when the

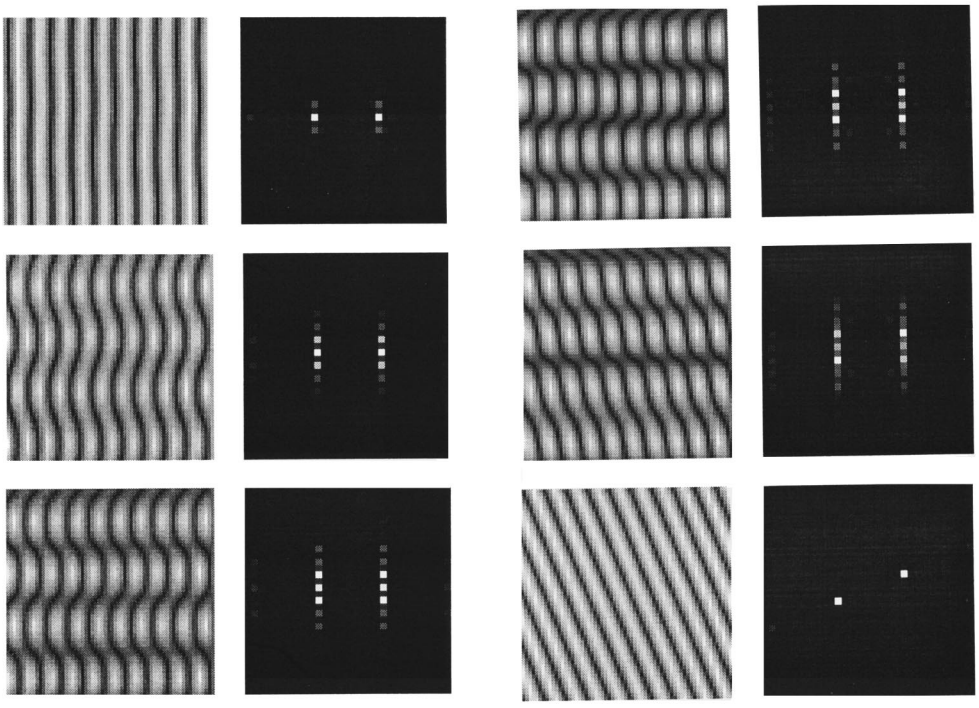

FIG. 5. Unstable zigzag for $\Delta_1 = -3$ and $p = 0.75$. (left) the series of spatial distributions of field intensity, (right) their corresponding 2D spatial Fourier spectra. The other parameters are as in Fig. 3. The time interval between the plots is $\Delta\tau = 28$. The dimension of the spatial grid is 32×32 pixels.

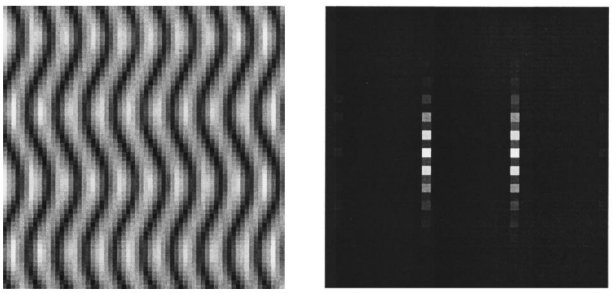

FIG. 6. Stable zigzag for $\Delta_1 = -2.2$, and $p = 0.75$. (Left) the spatial distribution of field intensity. (Right) its corresponding spatial Fourier spectra. The rest of the parameters as in Fig. 3. Note, however, that rolls with a different value of vector k have been analyzed in this 2D case, which results in a different value for the resonant signal detuning $\Delta_1 = -1.85$. The dimension of the spatial grid is 32×32 pixels.

higher roll components fall inside the instability ring which in its turn requires the initial roll to be close to resonance.

Our numerical calculations support this conclusion. For instance, the unstable zigzagged roll in Fig. 5 was obtained for an initial wave number K more off-resonant than that corresponding to the stable zigzagged roll in Fig. 6 (see captions). However, the boundary of the stability of the zigzag has not been calculated precisely, because of the drastical slowing down of the zigzag decay processes close to the expected boundary, and as a consequence the increasing computer time consumption.

B. Price hexagons (hexagons through zero-mode coupling)

As shown by Price [14(a)] and extended by Dewell *et al.* [14(b)] a system with a purely cubic nonlinearity, such as the Swift-Hohenberg model, can also support stable hexagons. These hexagons consist of three roll components at mutual angles of $2\pi/3$, plus a non-null plane-wave (zero-mode) component. The presence of the plane wave creates the squared nonlinearity necessary for supporting the mutual interaction of the roll components in the hexagons [1].

In order to obtain these hexagons one must necessarily seed them into the initial conditions for the numerical calculations. Our numerical simulations starting from random initial distributions lead to the excitation of rolls, because only the resonant spatial wave numbers survive in the initial stage of the linear growth.

We investigated numerically the stability of these Price hexagons. Figure 7 shows that the hexagons can coexist together with the rolls in DOPO for a sufficiently large range of the pump and detuning values. The domain of bistability between both patterns becomes smaller as the pump is decreased, and eventually disappears for a small enough pump, leaving only rolls in this case, in agreement with [14].

We investigated in more detail the roll-hexagon competition by varying the signal detuning. As Fig. 7 indicates the resonant signal detuning Δ_1 for hexagons (that for which the pattern reaches its maximum intensity) is shifted with respect to that for rolls. The reason for this resonance shift for hexagons is the presence of the zero mode: this mode requires a not very depressed gain in order to grow up, which is produced by bringing the detuning Δ_1 closer to zero.

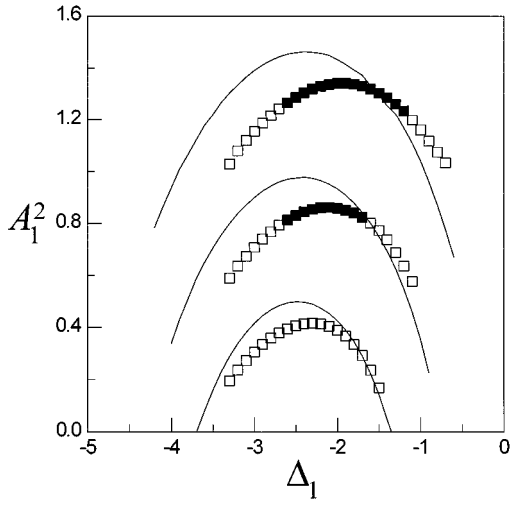

FIG. 7. Total intensity of numerically calculated hexagonal patterns (squares), and rolls (solid line), as a function of the signal detuning. The empty (filled) squares indicate unstable (stable) hexagons. The values of the pump parameter p are 0.5, 1, and 1.5 from bottom to top. The rest of the parameters are $a_1 = 0.004$, $a_0 = a_1/2$, $\Delta_0 = 0$, and $\gamma_0 = \gamma_1 = 1$.

By varying the signal detuning the Price hexagons lose their stability against the rolls. One scenario of the substitution of hexagons by rolls for a detuning larger (smaller in absolute value) than the resonant one for hexagons is illustrated by the series of plots in Fig. 8. We note that the hexagons lose their stability with respect to a roll with a smaller value of the spatial wave number K than that of the hexagon (compare the first and the last plots in Fig. 8). When the hexagons are detuned towards smaller values of signal detuning (larger in absolute value), then they lose their stability with respect to one of the roll components already present in the hexagon.

The series of plots in Fig. 8 may be viewed as one of the instability scenarios of the hexagon pattern. The hexagons, being more complicated than rolls, possibly contain also a richer family of instabilities. However, the detailed analysis of the instabilities of hexagons falls outside the scope of the present paper.

C. Nonlinear resonance

As has been discussed in Sec. III both DOPO and DFWM contain nonlinear resonances. We have checked the form of the nonlinear resonance numerically. For this purpose we fixed the number of stripes in the roll pattern in the integration domain (thus fixing a constant value of the vector K) by seeding a particular roll pattern in the initial distribution for the signal wave, as we have done in the previous numerics. The interactive interface for numerical programs allowed us to vary the values of the pump E and the detuning Δ_1 during the calculations, which enabled us to find not only the stable but also the unstable branches of the resonance curve. The numerical integration was performed without perturbing the fields in order to avoid possible instabilities of the rolls. In the following two subsections we show the results obtained both in DOPO and DFWM.

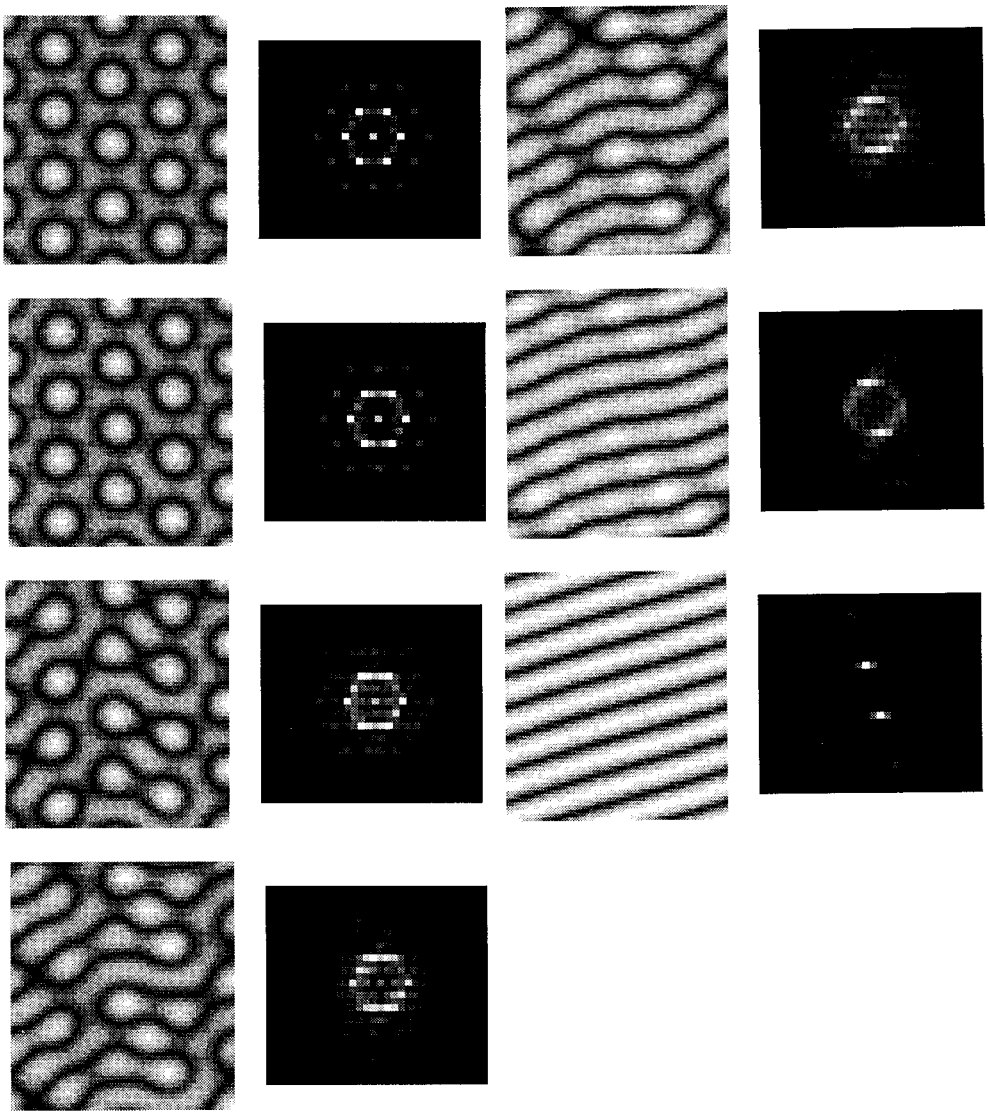

FIG. 8. The scenario of the instability of hexagons for $p=1$, $\Delta_1=-1.25$ and the rest of the parameters as in Fig. 7. The time interval between first and last plot is $\Delta\tau=170$ and the plots are equidistant in time. The dimension of the spatial grid is 32×32 pixels.

1. Nonlinear resonance in DOPO

As discussed in Sec. III A rolls in DOPO are described by Eq. (36). The behavior of the intensity of these rolls is clearly influenced by the nonlinear resonance, as shown in Fig. 1(b). Particularly Eq. (37b) shows that the roll whose intensity is maximum for a given pump p has a wave number k_0+k_{NLR}. This means that a roll of fixed wave number K in the numerical integrations will reach its maximum intensity at a signal detuning value Δ_1^{NLR} given by $K=K_0+K_{\mathrm{NLR}}$, with $K_{\mathrm{NLR}}=k_{\mathrm{NLR}}/\sqrt{a_1}$ and $K_0=\sqrt{(-\Delta_1/a_1)}$ [due to the normalization (2) of transverse variables used in the theoretical treatment]. Since k_{NLR} is small, as has been assumed in the derivation of the amplitude equations for rolls, Eq. (36), we can write $K^2\cong K_0^2+2K_0K_{\mathrm{NLR}}$ which, making use of Eq. (37b) yields

$$\Delta_1^{\mathrm{NLR}}=p[(2+\alpha)/(2+\alpha^2)]\Delta_0-a_1K^2. \tag{43}$$

This means that the roll of wave number K is resonant for signal detuning values that grow linearly with pump p and pump detuning Δ_0. The previous reasoning does not take into account that α is both Δ_0- and Δ_1-dependent [Eq. (34b)]. Nevertheless, α does not vary sensitively unless large variations of the detunings are made.

Figure 9 displays the resonance curves for DOPO on the plane $\langle\Delta_1,A_1^2\rangle$ for different values of the pump. The resonance curves are tilted as expected. The numerical results (symbols) fit well with those obtained from Eq. (36) (solid lines) even for pump values far beyond the assumptions made in deriving Eq. (36): for instance, $p=0.2$ $[\varepsilon\cong 0.44=O(1)]$ in the upper curve. This indicates the structural robustness of the amplitude equation for DOPO.

One of the consequences of the nonlinear resonance is the appearance of bistability in DOPO between the roll solution at a given K and the trivial solution for sufficiently large values of the pump. Nevertheless, any small perturbation will destabilize the trivial solution and a roll pattern with the appropriate wave number will grow.

The other consequence is that the boundaries of the Eckhaus and zigzag instabilities are expected to be also tilted, which can initiate long and complicated transients. The terms of differential nonlinearity in Eq. (34) can also lead to different instabilities of rolls with respect to the SHE case, as

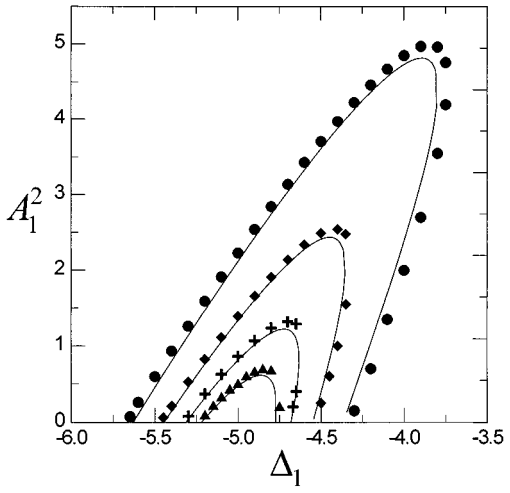

FIG. 9. Total intensity of the signal field for a one-dimensional roll pattern of spatial frequency $K=10\pi$ as a function of the signal detuning Δ_1 for nonzero pump detuning $\Delta_0=5$ (nonlinear resonance). The values of the pump parameter p are 0.025, 0.05, 0.1, and 0.2 from bottom to top. The analytical results [obtained from Eq. (36)] are represented by the solid lines. The rest of the parameters are $a_1 = 0.005\,065$, $a_0=a_1/2$, and $\gamma_0=\gamma_1=1$.

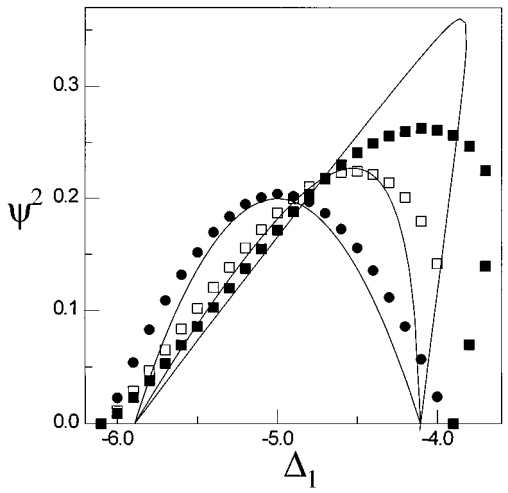

FIG. 10. Numerical (symbols) and analytical (lines) nonlinear resonance curves for DFWM, for a roll pattern of spatial frequency $K=10\pi$, and different pump detuning values: $\Delta_0=0$ (circles), $\Delta_0=1$ (open squares), and $\Delta_0=1.5$ (filled squares). The analytical results come from Eq. (38). The rest of the parameters are $p=0.2$, $a_1=a_0=0.005\,065$ and $\gamma_0=\gamma_1=1$. Note that the normalized intensity ψ^2 of the signal field is plotted here $[\psi^2=A_1^2/(1+\Delta_0^2)]$, differently from Fig. 9 for the DOPO case, for the sake of better comparing the curves.

skew-varicose or others [1]. We also note that the terms causing the nonlinear resonance are nonvariational ones: the modified SHE Eq. (24) does not posses an action integral, differently from the SHE [1]. Consequently, one can also expect dynamical solutions (like periodic or maybe chaotic regimes) in the modified SHE, differently from the SHE case where all the end solutions are stationary and correspond to local or global potential minima.

2. Nonlinear resonance in DFWM

As already commented, the differences between DOPO and DFWM are expected to occur for large pump detunings, when the nonlinear resonance appears, as has been illustrated in Figs. 1(b) and 2(a).

We have obtained numerically the nonlinear resonance curves for DFWM in order to check the validity limits of Eq. (39). Figure 10 displays a family of nonlinear resonances of the roll pattern for three different (moderate) values of the pump detuning Δ_0, corresponding to both numerical (symbols) and analytical results (lines). In this case the agreement is not so good as in the DOPO case but it is still reasonable, especially for the smaller values of the pump detuning (see caption). Note that the inclination angles of the resonance curves are roughly inversely proportional to the pump detuning exactly as predicted in the DOPO case [$\psi^2_{\max}/k_{\mathrm{NLR}}$ from Eqs. (37)]. Contrarily, the maximum value of the amplitude of the rolls was found to be strongly dependent on the pump detuning, differently from the DOPO case in which this value depends only slightly on Δ_0.

For larger values of the pump detuning also qualitative differences between DOPO and DFWM appear. This is illustrated in Fig. 11 which has been calculated for $\Delta_0=2$. We note that the whole resonance curve could not be traced. Also the presence of another branch of solutions is shown. By increasing detuning from approximately -6 the branch of (roll) solutions could be followed up to a value of around -3.8. At this detuning value this branch of solutions became unstable and a sudden transition to a different branch of solutions (open squares in Fig. 11) was observed, a domain of bistability existing between the two branches of solutions.

The appearance of a new branch of solutions (which actually seems to have exactly the same spatial distribution as the usual rolls) is impossible for the SHE as well as for the DOPO equations, and signals the end of the similarity between the DOPO and DFWM. The new branch of solutions appeared for a value of the pump detuning between 1.5 and 2 in our numerical calculations. This can be related to the breakdown of the amplitude equation for rolls in DFWM that

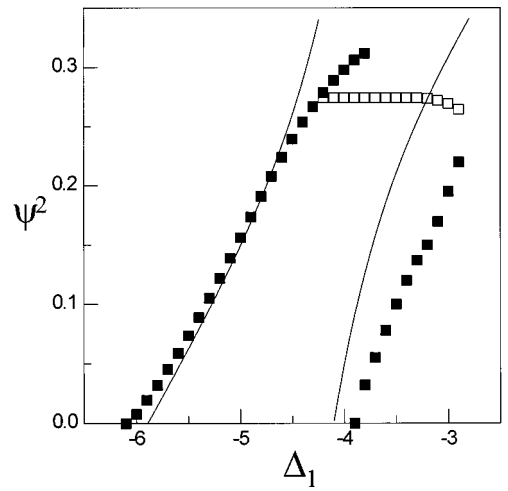

FIG. 11. As Fig. 10 but for $\Delta_0=2$. The nonlinear resonance curve is broken (compare with Fig. 10), and a new stable solution branch (open squares) appears.

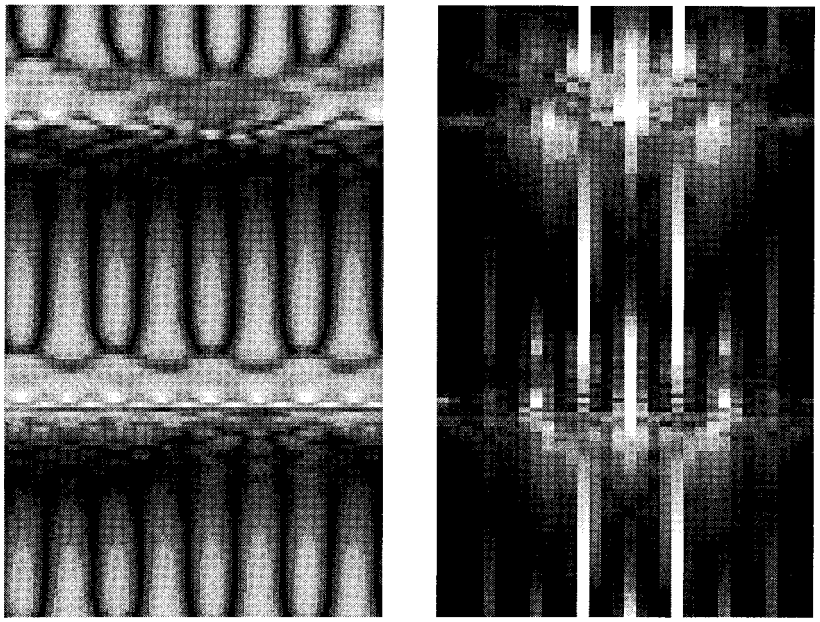

FIG. 12. Temporal evolution of the spatial distribution of the signal field (left) and of its spatial Fourier spectrum (right) in the DFWM chaotic regime. The parameters are $p=0.27$, $\Delta_0=-5$, $\Delta_1=-3$, and the rest of the parameters as in Fig. 10. The time changes from top to bottom over $\Delta t=2.5$ and the spatial scale (horizontal) has 128 pixels.

was noted in Fig. 2(a) and can be seen in Figs. 10 and 11: as Δ_0 is increased from 1.5 (upper curve in Fig. 10) to 2 (Fig. 11), the resonance curve gets broken.

Which is the behavior of DFWM for parameters far away from the range of validity of its OPE? The answer to this question falls outside the scope of the present paper and deserves a separate study. Our preliminary numerical calculations show the following features, different from those expected from the analysis of the OPE and amplitude equation of DFWM: (i) stationary rolls with an additional zero component in the 1D case; (ii) coexistence of two rolls with two different spatial wave numbers in the 1D case; (iii) Price hexagons in the 2D case that do not coexist with the rolls but win in a roll-hexagon competition; and (iv) oscillatory regimes involving different spatial degrees of freedom.

As an example, Fig. 12 displays a space-time plot of a nonstationary regime of DFWM in the 1D case, after transients have decayed. This nonstationary regime involves irregular spatiotemporal oscillations, resembling the spatiotemporal intermittency.

V. CONCLUSIONS

Transverse pattern formation in degenerate optical parametric oscillation (DOPO) and degenerate four-wave mixing (DFWM) have been considered. For small signal detuning the Swift-Hohenberg equation (SHE) has been shown to describe both systems. Nevertheless, this isomorphism breaks down for large values of the pump detuning. This manifests itself through a modification of the SHE involving the appearance of higher-order nonlinearities, that are different for DOPO and DFWM. The role played by these extra terms is to produce a nonlinear resonance in both systems. In the case of DFWM the modified SHE shows a pathological behavior since it does not saturate for large values of the intensity of the signal field, far above the generation threshold. For positive signal detuning the real Ginzburg-Landau equation is obtained for both DOPO and DFWM.

Amplitude equations for roll patterns have been obtained from the microscopic equations in both systems, under a variety of different scales for the detuning parameters. Particularly, for large pump detuning the amplitude equation contains terms corresponding to the nonlinear resonance predicted by the modified SHE. An interpolating amplitude equation has been given, which covers all the analyzed cases, and, in particular, the amplitude equation obtained from the modified SHE if pump detuning is made large. These interpolated amplitude equations are different for DOPO and DFWM.

In order to test the analytical predictions numerical integration of the microscopic equations have been carried out. A good agreement has been found, even for parameter values far from those considered in the theoretical analysis. The roll instabilities (Eckhaus and zigzag), the hexagonal patterns with an additional zero component (Price hexagons), and the competition between these hexagons and rolls have also been analyzed. The numerical analysis has also evidenced the existence of nontrivial dynamical patterns in DFWM, which will be studied in the future.

Note added in proof. Recently a paper by H. Sakaguchi [Prog. Theor. Phys. **86**, 759 (1991)] has come to our knowledge. In it the post-zigzag states of the SHE are investigated. He shows that for small (large) k the zigzag is stable (unstable). This is in agreement with our calculations.

ACKNOWLEDGMENTS

We gratefully acknowledge Massimo Brambilla for sharing Ref. [5] with us prior to its publication, Gian-Luca Oppo for informing us about his calculations on resonant structures in DOPO, and J. M. Ajenjo for help in some preliminary calculations. This work has been supported by the Spanish DGICYT through Contract No. PB92-0600-C03-02. K.S. acknowledges a grant from the Generalitat Valenciana (Valencian Government), and financial support from the Deutsche Forschungsgemeinschaft.

APPENDIX A

In this appendix we discuss briefly the derivation of OPE's for the case of finite positive detuning. With respect to the linear stability analysis, substitution of (9b) into (11) shows that the largest eigenvalue is of order ε^2 for k^2 of order ε. Then, in this case the spatial part scales as

$$\nabla^2=\varepsilon^2\nabla_2^2 \tag{A1}$$

and Δ_1 can be $O(1)$. The scaling is applicable to both DOPO and DFWM.

For DOPO the order-parameter equation for finite positive detuning reads, to leading order in ε,

$$\partial_\tau\overline{Y}=E_0p\overline{Y}-2E_0(1-E_0)(1-\Delta_0\Delta_1)\overline{Y^3}+\Delta_1\nabla^2\overline{Y}, \tag{A2}$$

with

$$p=E-E_0, \tag{A3a}$$

and

$$Y=[\Delta_1+i(1-E_0)]\overline{Y}. \tag{A3b}$$

Equation (A2) is the real Ginzburg-Landau equation. Notice that this equation is not valid when $\Delta_0\Delta_1>1$, since in this case the cubic term becomes positive and the solutions diverge. This fact is due to the existence of bistability of the homogeneous solutions close to threshold that just occurs for $\Delta_0\Delta_1>1$.

For DFWM the order-parameter equation for finite positive detuning reads

$$\partial_\tau\overline{Y}=2E_0^2p\overline{Y}-4E_0^2(E_0^2-1)(1-\Delta_0\Delta_1)\overline{Y^3}+\Delta_1\nabla^2\overline{Y}, \tag{A4}$$

with p given by Eq. (A3a), and

$$Y=[\Delta_1+i(1-E_0^2)]\overline{Y}, \tag{A5}$$

which is isomorphic to Eq. (A2), as can be seen by making $\overline{Y}\to\overline{Y}/\sqrt{2}$ and $p\to p/2$ in Eq. (A4).

APPENDIX B

In this appendix we derive the amplitude equation for rolls in DOPO in the case of pump and signal detuning of order one. For that we make an expansion of Eqs. (4) assuming an increase of the pump over threshold of order ε^2, Eq. (10), applying the expansion of the Laplacian operator given in Eqs. (31), and using the expansion (15) for the fields, but now we impose

$$Y_1=B(u,v)e^{ik_0x}+B^*(u,v)e^{-ik_0x}. \tag{B1}$$

At order ε we find $X_1=0$. At order ε^2 we find

$$[L_0+2i\gamma(1+i\Delta_0)]X_2=-2i\gamma(1+i\Delta_0)Y_1^2, \tag{B2a}$$

$$[1+i(\Delta_1-L_0)]Y_2=Y_2^*+iL_1Y_1, \tag{B2b}$$

which by using Eq. (B1) give the solutions

$$X_2=-\left[2|B|^2+\frac{1+i\Delta_0}{1+i(\Delta_0-2\Delta_1/\gamma)}(B^2e^{2ik_0x}+\text{ c.c.})\right], \tag{B3a}$$

$$Y_2=Y_2^{(+1)}e^{ik_0x}+Y_2^{(-1)}e^{-k_0x}, \tag{B3b}$$

with

$$Y_2^{(+1)}=Y_2^{(-1)}*+iL_1B. \tag{B3c}$$

Finally, at order ε^3 we find

$$\partial_\tau Y_1=E_2Y_1+\tfrac{1}{2}[(1-i\Delta_0)X_2+(1+i\Delta_0)X_2^*]Y_1 +\tfrac{1}{2}iL_1(Y_2-Y_2^*)+\tfrac{1}{2}i(L_0-\Delta_1)(Y_3-Y_3^*), \tag{B4}$$

which evaluated at the frequency k_0 leads to the amplitude equation for rolls that read

$$\partial_\tau B(u,v)=E_2B-(2+\alpha^2)|B|^2B-\tfrac{1}{2}L_1^2B \tag{B5}$$

with $\alpha=\sqrt{(1+\Delta_0^2)/[1+(\Delta_0-2\Delta_1/\gamma)^2]}$.

APPENDIX C

In this appendix we derive the amplitude equation for rolls in DOPO in the case of large pump and signal detuning. Thus we put

$$\Delta_1=\varepsilon^{-1}\delta_1, \tag{C1a}$$

$$\Delta_0=\varepsilon^{-1}\delta_0, \tag{C1b}$$

which implies

$$k_0=\varepsilon^{-1/2}\overline{k_0}, \tag{C1c}$$

apply the expansion of the Laplacian operator given in Eq. (33) and proceed as in Appendix B, but now we put

$$Y_1=Be^{-i\overline{k}_0x_0}+B^*e^{-i\overline{k}_0x_0}. \tag{C2}$$

At order one we find $X_1=0$. At order ε we find

$$[L_{-1}-2\gamma\delta_0]X_2=2\gamma\delta_0Y_1^2, \tag{C3a}$$

$$(L_{-1}-\delta_1)Y_2=-i(Y_1-Y_1^*), \tag{C3b}$$

which by using Eq. (C2) give the solutions

$$X_2=-[2|B|^2+\alpha'(Be^{2ik_0x_0}+\text{ c.c.})], \tag{C4a}$$

$$Y_2=Y_2^{(+1)}e^{i\overline{k}_0x_0}+Y_2^{(-1)}e^{-i\overline{k}_0x_0}, \tag{C4b}$$

with

$$\alpha'=1/(1-2\delta_1/\gamma\delta_0). \tag{C4c}$$

Notice that X_2 is a real quantity.

At order ε^2 we find

$$(L_{-1}-2\gamma\delta_0)X_3=-2i\gamma(X_2+Y_1^2+2i\gamma\delta_0 Y_1Y_2), \tag{C5a}$$

$$(L_{-1}-\delta_1)Y_3=-i(Y_2-Y_2^*)-(L_1-\delta_0X_2)Y_1. \tag{C5b}$$

Solving Eq. (C5a) gives

$$X_3=X_3^{(+2)}e^{i2\overline{k}_0x_0}+X_3^{(0)}+X_3^{(-2)}e^{-2i\overline{k}_0x_0}, \tag{C6a}$$

with

$$X_3^{(+2)}=i\alpha'\left(\frac{1-\alpha'}{\delta_0}B+2iY_2^{(+1)}\right)B, \tag{C6b}$$

$$X_3^{(0)}=-2(BY_2^{(-1)}+B^*Y_2^{(+1)}), \tag{C6c}$$

$$X_3^{(-2)}=i\alpha'\left(\frac{1-\alpha'}{\delta_0}B^*+2iY_2^{(-1)}\right)B^*. \tag{C6d}$$

Equation (C5b) does not need to be solved for Y_3 since it will not appear in the solvability condition (see below). We only need to evaluate this equation at the frequency k_0. The result is

$$Y_2^{(+1)}-Y_2^{(-1)*}=iL_1B+i\delta_0(2+\alpha')|B|^2B. \tag{C7}$$

Finally, at order ε^3 we find

$$\begin{aligned}\partial_\tau Y_1=&E_2Y_1+X_2Y_1+\tfrac{1}{2}i(L_1+\delta_0X_2)(Y_2-Y_2^*)\\&-\tfrac{1}{2}i\delta_0(X_3-X_3^*)Y_1+\tfrac{1}{2}i(L_{-1}-\delta_1)(Y_4-Y_4^*),\end{aligned} \tag{C8}$$

which evaluated at the frequency $\overline{k_0}$ leads to the amplitude equation for rolls

$$\begin{aligned}\partial_\tau B(u,v)=&E_2B-(2+\alpha'^2)|B|^2B-\tfrac{1}{2}\delta_0^2(2+\alpha')^2|B|^4B\\&-\tfrac{1}{2}L^2B-\tfrac{1}{2}\delta_0[(2-\alpha')B^2L^*B^*+2\alpha'|B|^2LB\\&+(2+\alpha')L(|B|^2B)].\end{aligned} \tag{C9}$$

Now, let us simply comment that a third amplitude equation can be derived if we consider Δ_1 of order one and $\Delta_0=\varepsilon^{-1}\delta_0$. In this case one must apply the same scalings as in Appendix B but the one corresponding to pump detuning. The amplitude equation obtained in this way is the same as Eq. (C9) but replacing α' by 1. This is consistent since in this case $\Delta_0\gg\Delta_1$ and in this limit $\alpha'\to1$. This amplitude equation is the same that one obtains by starting directly with the OPE Eq. (24).

On the other hand, Eq. (C9) and Eq. (B5) do not connect completely. It is verified that $\alpha\to\alpha'$ when Δ_0 and Δ_1 are large but if both detunings are made of order one in Eq. (C9) one obtains Eq. (5) but with α' instead of α. Nevertheless, we can construct an interpolated equation by putting α instead α' in Eq. (C9), this equation [that is Eq. (34a)] being valid in all the three limits that have been considered.

APPENDIX D

In this appendix we derive the amplitude equation for rolls in DFWM in the case of pump and signal detuning of order one. The derivation follows the same lines as for the DOPO case (Appendix B).

At order ε we find $X_1=0$. At order ε^2 we find

$$[iL_0-\gamma(1+i\Delta_0)]X_2=\gamma(1+i\Delta_0)Y_1^2 \tag{D1}$$

and Eq. (B3b) which, by using Eq. (B1), give the solution

$$X_2=-\left[2|B|^2+\frac{1+i\Delta_0}{1+i(\Delta_0-4\Delta_1/\gamma)}(B^2e^{2ik_0x}+\text{c.c.})\right], \tag{D2}$$

and the same expression for Y_2 as in Appendix A.

Finally, at order ε^3 we find the same equation as for the DOPO case [Eq. (B4)] but replacing E_2 by $2E_2$, which evaluated at the frequency k_0 leads finally to the rolls' amplitude equation

$$\partial_\tau B(u,v)=2E_2B-2(2+\beta^2)|B|^2B-\tfrac{1}{2}L^2B \tag{D3}$$

with $\beta=\sqrt{(1+\Delta_0^2)/[1+(\Delta_0-4\Delta_1/\gamma)^2]}$. Notice that this equation is isomorphic to the corresponding one for DOPO.

APPENDIX E

In this appendix we derive the amplitude equation for rolls in DFWM in the case of large pump and signal detuning. Again we follow the same lines as for the DOPO (Appendix C).

At order one we find $X_1=0$. At order ε we find

$$[L_{-1}-\gamma\delta_0]X_2=\gamma\delta_0Y_1^2, \tag{E1}$$

and the same Eq. (C3b) that, by using Eq. (C2) give the solutions Eq. (C4b) and

$$X_2=-[2|B|^2+\beta'(Be^{2i\overline{k}_0x_0}+\text{c.c})], \tag{E2a}$$

with

$$\beta'=\frac{1}{1-4\delta_1/\gamma\delta_0}, \tag{E2b}$$

thus X_2 being a real quantity.

At order ε^2 we find

$$(L_{-1}-\gamma\delta_0)X_3=-i\gamma(X_2+Y_1^2-\delta_0^2X_2Y_1^2+2i\delta_0Y_1Y_2), \tag{E3a}$$

$$(L_{-1}-\delta_1)Y_3=-i(Y_2-Y_2^*)-(L_1-2\delta_0X_2)Y_1. \tag{E3b}$$

Solving Eq. (E3a) gives

$$\begin{aligned}X_3=&X_3^{(+4)}e^{i4\overline{k}_0x_0}+X_3^{(+2)}e^{i2\overline{k}_0x_0}+X_2^{(0)}+X_3^{(-2)}e^{-2i\overline{k}_0x_0}\\&+X_3^{(-4)}e^{-i4\overline{k}_0x_0},\end{aligned} \tag{E4a}$$

with

$$X_3^{(+2)}=i\beta'\left(\frac{1-\beta'}{\delta_0}B+2iY_2^{(+1)}+2\delta_0(1+\beta')|B|^2B\right)B, \tag{E4b}$$

$$X_3^{(0)}=-2(BY_2^{(-1)}+B^*Y_2^{(+1)})+2i\delta_0(2+\beta')|B|^4, \tag{E4c}$$

$$X_3^{(+2)}=i\beta'\left(\frac{1-\beta'}{\delta_0}B^*+2iY_2^{(-1)}+2\delta_0(1+\beta')|B|^2B^*\right)B^*. \tag{E4d}$$

As in the DOPO case, Eq. (E3b) does not need to be solved for Y_3 since it will not appear in the solvability condition (see below). The same occurs with $X_3^{(+4)}$ and $X_3^{(-4)}$. We only need to evaluate this equation at the frequency $\overline{k_0}$. The result is

$$Y_2^{(+1)}-Y_2^{(-1)*}=iL_1B+2i\delta_0(2+\beta')|B|^2B. \tag{E5}$$

At order ε^3 we find the equation

$$\begin{aligned}\partial_\tau Y_1=&2E_2Y_1+2X_2Y_1-\delta_0^2X_2^2Y_1\\&+\tfrac{1}{2}i(L_1+2\delta_0X_2)(Y_2-Y_2^*)-i\delta_0(X_3-X_3^*)Y_1\\&+\tfrac{1}{2}i(L_{-1}-\delta_1)(Y_4-Y_4^*)+\tfrac{1}{2}i[\partial_\tau-2E_2-2X_2\\&-\delta_0^2X_2^2-2i\delta_0X_3](L_{-1}-\delta_1)Y_2,\end{aligned} \tag{E6}$$

which evaluated at the frequency $\overline{k_0}$ leads finally to the amplitude equation for rolls that read

$$\begin{aligned}\partial_\tau B(u,v)=&2E_2B-2(2+\beta'^2)|B|^2B-4\delta_0^2(1+\beta')|B|^4B\\&-\tfrac{1}{2}L_1^2B-\delta_0[(2-\beta')B^2L_1^*B^*+2\beta'|B|^2L_1B\\&+(2+\beta')L_1(|B|^2B)].\end{aligned} \tag{E7}$$

Here the same considerations that were made in the DOPO case with respect to the interpolation must be applied.

[1] M. C. Cross and P. C. Hohenberg, Rev. Mod. Phys. **65**, 851 (1993).

[2] P. Coullet, L. Gil, and F. Rocca, Opt. Commun. **73**, 403 (1989).

[3] G. L. Oppo, M. Brambilla, and L. A. Lugiato, Phys. Rev. A **49**, 2028 (1994).

[4] G. L. Oppo, M. Brambilla, D. Camesasca, A. Gatti, and L. A. Lugiato, J. Mod. Opt. **41**, 1151 (1994).

[5] M. Brambilla, D. Camesasca, and G. L. Oppo (unpublished).

[6] G. L. Oppo (private communication).

[7] L. A. Lugiato and G. Grynberg, Europhys. Lett. **29**, 675 (1995).

[8] K. Staliunas, J. Mod. Opt. **42**, 1261 (1995).

[9] P. Mandel, M. Georgiou, and T. Erneux, Phys. Rev. A **47**, 4277 (1993).

[10] V. J. Sánchez-Morcillo and G. J. de Valcárcel, Quantum Semiclass. Opt. (to be published).

[11] J. Swift and P. C. Hohenberg, Phys. Rev. A. **15**, 319 (1977).

[12] C. M. Savage and D. F. Walls, J. Opt. Soc. Am. B **4**, 1514 (1987).

[13] P. Manneville, *Dissipative Structures and Weak Turbulence* (Academic Press, San Diego, 1990).

[14] (a) C. B. Price, Phys. Lett. A **194**, 385 (1994); (b) G. Dewel, S. Métens, M'F. Hilaly, P. Borckmans, and C. B. Price, Phys. Rev. Lett. **74**, 4647 (1995).

[15] L. Kramer, H. R. Schober, and W. Zimmermann, Physica D **31**, 212 (1988).